Inorganic Chemistry

pubs.acs.org/IC

Article

Phosphine Ligand Binding and Catalytic Activity of Group 10−14 Heterobimetallic Complexes

Carena L. Daniels,[⊥] Eunbyeol Gi,[⊥] Benjamin A. Atterberry, Rafael Blome-Fernández, Aaron J. Rossini, and Javier Vela*

Cite This: *Inorg. Chem.* 2022, 61, 6888−6897

Read Online

ACCESS | Metrics & More | Article Recommendations | Supporting Information

ABSTRACT: Heterobimetallic complexes have attracted much interest due to their broad range of structures and reactivities as well as unique catalytic abilities. Additionally, these complexes can be utilized as single-source precursors for the synthesis of binary intermetallic compounds. An example is the family of bis(pyridine-2-thiolato)dichloro-germanium and tin complexes of group 10 metals (Pd and Pt). The reactivity of these heterobimetallic complexes is highly tunable through substitution of the group 14 element and the neutral ligand bound to the transition metal. Here, we study the binding energies of three different phosphorous-based ligands, PR_3 (R = Bu, Ph, and OPh) by density functional theory and restricted Hartree−Fock methods. The PR_3 ligand-binding energies follow the trend of $PBu_3 > PPh_3 > P(OPh)_3$, in agreement with their sigma-bonding ability. These results are confirmed by ligand exchange experiments monitored with ^{31}P NMR spectroscopy, in which a weaker binding PR_3 ligand is replaced with a stronger one. Furthermore, we demonstrate that the heterobimetallic complexes are active catalysts in the Negishi coupling reaction, where stronger binding PR_3 ligands inhibit access to an active site at the metal center. Similar strategies could be applied to other complexes to better understand their ligand-binding energetics and predict their reactivity as both precursors and catalysts.

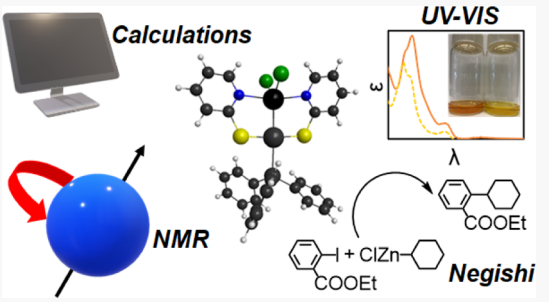

INTRODUCTION

Pincer complexes are structurally diverse inorganic molecules with a distinct balance of stability and reactivity, often resulting in unique catalytic activity. Pincer complexes are widely used as catalysts for Mizoroki−Heck, Suzuki−Miyaura, Sonogashira, Hiyama, and Negishi coupling reactions, among others.[1−3] For example, Pd pincer complexes bearing S-donor atoms, commonly referred to as SCS or SNS complexes—depending on the specific central donor atom—have been studied for the Mizoroki−Heck cross coupling—*i.e.*, the reaction between an unsaturated halide or triflate and an alkene, the Suzuki−Miyaura cross coupling—between a boronic acid and an organohalide,[4] and C−S diarylthioetherification−the reaction between a disulfide and an organohalide.[5] Other examples include bis(*N*-heterocyclic thione) (NHT) Pd complexes as catalysts for the Suzuki−Miyaura, Mizoroki−Heck, and Sonogashira cross-coupling reactions—the latter between a terminal alkyne and an aryl- or vinyl halide.[6]

Recently, hetero-element pincer ligands built around heavier main group elements and their complexes with Ni, Pd, or Pt have attracted interest because of their unique bonding and reactivity. For example, PAlP pincer complexes of Ni have been synthesized and studied for C−X, H−H, and C−H bond activation and intramolecular aryl transfer.[7] PTrP (Tr = Al, Ga, or In) pincer complexes of Pd have been studied as catalysts for the hydrosilylation of CO_2.[8] PSiP, PSiN, and NSiN pincer complexes have been studied for Si−H bond activation, C−H borylation of arenes, hydrocarboxylation of allenes, dehydrogenative borylation, fluorosilane activation, and hydroborylation of CO_2.[9−12] A PGeP pincer complex of Pd has been studied as a catalyst for the hydrocarboxylation of allenes[13] and the hydrometallation of ethylene.[14] The heterobimetallic bonding interaction between the group 14 element (E = Ge or Sn, sometimes referred to as "tetrel") and Ni, Pd, or Pt in SES and PEP complexes has been studied (E = group 14 element).[15−23] PEP (E = Si, Ge, and Sn) complexes of Pd were demonstrated to be active catalysts for a reductive aldol-type reaction.[24] PSnP complexes of group 10 metals undergo Sn−Cl bond activation and alkyl transfer.[25] PSbP complexes of Pd act as water compatible F^- ion sensors.[26] PSbP complexes of Pt undergo photoreductive elimination of Cl in both solution and in the solid state.[27] Some of these complexes have also been applied to alkyne activation, enyne cyclization, intramolecular hydroarylation, and the catalytic addition of pyrrole

Received: January 20, 2022
Published: April 28, 2022

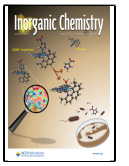

https://doi.org/10.1021/acs.inorgchem.2c00229
Inorg. Chem. 2022, 61, 6888−6897

and thiophenes to alkynes.[28−31] PBiP complexes of group 10 metals were also reported.[32−35]

Another emerging application of heterobimetallic complexes supported by hetero-element pincers is their use as single-source precursors to intermetallic nanocrystals.[36−38] In a recent study, varying the monodentate donor ligands (phosphine or phosphite) bound to SES complexes leads to different nanocrystalline products upon thermolysis.[36] This suggests that the reactivity of the heterobimetallic [EPd] core can be fine-tuned by ligand substitution.[36] This observation bears promise beyond the use of similar complexes as molecular precursors as these could also become a potentially tunable class of homogeneous catalysts. Nonetheless, the use of such heterobimetallic complexes as catalysts is relatively underexplored.

In this study, we use a combination of computational and experimental methods to measure the relative binding affinity of different phosphorous-based ligands on the heterobimetallic [EM] core in a family of bis(pyridine-2-thiolato)dichloro−element complexes of group 10 metals. These have the general formula $Cl_2E(\mu\text{-PyS})_2M\text{-}PR_3$, where E = Ge or Sn, M = Pd or Pt, and R = Ph, OPh, or Bu (Figure 1). Using complementary

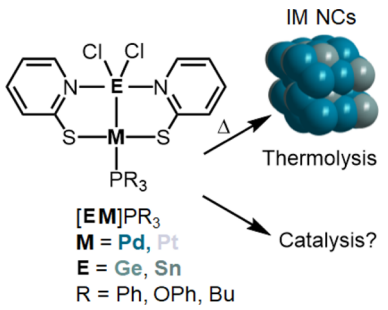

Figure 1. Bis(pyridine-2-thiolato)dichloro-group 14 complexes of group 10 metals and their demonstrated or potential applications. [EM] denotes the heterobimetallic $Cl_2E(\mu\text{-PyS})_2M$ core. IM NCs denotes the intermetallic nanocrystals.

computational methods, we estimate the relative strength of the Pd−PR_3 binding interaction in these complexes. Using solution-phase ^{31}P NMR and UV−vis absorption spectroscopies, we study the exchange of the different tertiary phosphine and phosphite ligands onto the heterobimetallic $[EPd]PR_3$ core. Finally, we demonstrate that the heterobimetallic complexes are active catalysts in the Negishi coupling reaction between ethyl-*o*-iodobenzoate and cyclohexyl zinc chloride.

RESULTS AND DISCUSSION

M−PR_3-Binding Energy Calculations. A previous study of $[SnPd]PR_3$ complexes bearing different phosphorous-based ligands—$P(OPh)_3$, PPh_3, and PBu_3—showed thermolysis resulted in the formation of different intermetallic nanocrystal phases—$Pd_{20}Sn_3$, Pd_3Sn_2, and Pd_2Sn, respectively ("IM NCs" in Figure 1).[36] To better understand the effect of the exact phosphine or phosphite ligand binding on the chemistry and reactivity of the heterobimetallic complexes, we computationally calculated the binding energies—formally, heterolytic bond dissociation energies (BDEs)—and enthalpies of the $[EM]PR_3$ complexes (E = Ge or Sn and M = Pd or Pt), according to Scheme 1. Calculations were performed using density functional theory (DFT) with the popular B3LYP

Scheme 1. Hypothetical Ligand Dissociation Reaction Used to Calculate PR_3-Binding Affinities in Heterobimetallic $[EM]PR_3$ Complexes (See the Supporting Information)

$$[SnPd]PPh_3 \longrightarrow [SnPd] + PPh_3$$

functional and, for comparison, with restricted Hartree−Fock (RHF) utilizing the MIDI basis set (see the methods section). We started by optimizing the geometry of the $[EPd]PR_3$ complex, followed by breaking the coordination (dative) M−P bond to create two separate fragments, [EM] and free PR_3. Bond energetics were calculated after geometry optimization. In each case, the M−P bond enthalpy (ΔH) and Gibbs free energy (ΔG) were calculated as the difference between the two fragments and the initial complex (Table 1).

Table 1. Calculated PR_3-Binding Affinity Energies (ΔG) and Enthalpies (ΔH) for Heterobimetallic Complexes

complex[a]	ΔG (kcal/mol)[b]	ΔH (kcal/mol)[c]
Restricted Hartree−Fock with MIDI Basis Set		
$[GePd]P(OPh)_3$	13.57	25.11
$[GePd]PPh_3$	14.87	27.59
$[GePd]PBu_3$	21.13	32.99
$[SnPd]P(OPh)_3$	9.57	20.57
$[SnPd]PPh_3$	10.10	22.82
$[SnPd]PBu_3$	15.81	27.46
$[SnPt]PPh_3$	11.19	24.16
DFT with B3LYP, SBKJC Basis Set		
$[GePd]P(OPh)_3$	7.83	21.93
$[GePd]PPh_3$	12.51	26.75
$[GePd]PBu_3$	19.55	31.82
$[SnPd]P(OPh)_3$	7.00	20.55
$[SnPd]PPh_3$	10.47	25.39
$[SnPd]PBu_3$	16.47	31.43
$[SnPt]PPh_3$	1.66	15.31

[a][EM] denotes $Cl_2E(\mu\text{-PyS})_2M$ core (E = Ge or Sn and M = Pd or Pt). [b]$\Delta G = (G_{[EM]} + G_{PR3}) - G_{[EM]PR3}$. [c]$\Delta H = (H_{[EM]} + H_{PR3}) - H_{[EM]PR3}$.

Both DFT (B3LYP) and RHF (MIDI) computational methods afford similar trends. For each EPd series—GePd or SnPd—the BDEs (ΔG or ΔH) increase in the order: $P(OPh)_3 < PPh_3 < PBu_3$. In other words, PR_3 ligand binding is the weakest for the best π-acceptor, $P(OPh)_3$, and strongest for the best σ-donor, PBu_3. In both cases, the values are consistently larger—by *ca.* 5 kcal/mol—for the GePd complexes than that for the SnPd complexes, indicating that PR_3 ligand binding may be stronger for Ge-based complexes than that for analogous Sn-based complexes. This difference is hard to rationalize solely based on the small electronegativity differences (χ_P 2.01 for Ge vs 1.96 for Sn) or the higher Lewis acidity of tin versus germanium chlorides (see LMO analysis below).[39] Overall, individual PR_3 binding enthalpies (ΔH) range from 20.6 to 33.0 kcal/mol and free energies (ΔG) range from 7.0 to 21.1 kcal/mol (Figure 2).

E−M Bonding and Orbital Calculations. In frontier orbital analysis, the computationally less expensive RHF method was used to draw the highest occupied molecular orbitals (HOMOs) and lowest unoccupied molecular orbitals (LUMOs) in [EPd] complexes containing the three phosphorous-based ligands—see the Supporting Information available. In all complexes, the HOMOs are localized along

https://doi.org/10.1021/acs.inorgchem.2c00229
Inorg. Chem. 2022, 61, 6888−6897

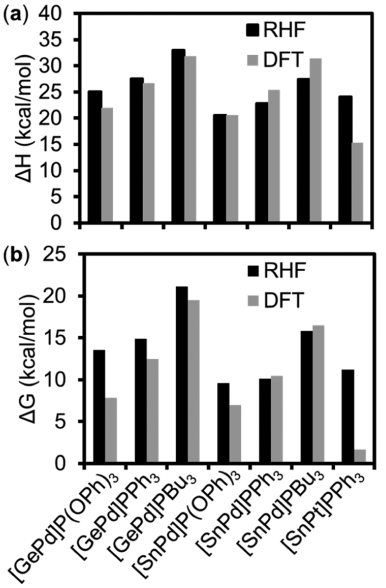

Figure 2. Calculated PR_3-binding affinity enthalpies (ΔH, a) and energies (ΔG, b) in $[EM]PR_3$ complexes using two different computational levels of theory (see the methods section).

the S−Pd−S axis, with contributions from the Pd d_{xz} and S p_z orbitals. The HOMOs also extend onto the pyridine ring arms of the pincer ligands, with each ring displaying a node on its π-electron density. Interestingly, the HOMOs lack contributions from the group 14 element or the PR_3 ligand. In contrast, the LUMO orbitals extend through the whole [EPd] framework, across both S−Pd−S and E-Pd-P axes (see the Supporting Information).

Localized molecular orbital (LMO) analysis was carried out with GAMESS by the RHF/MIDI and Edmiston and Ruedenberg method to reveal E-Pd bonding features of $[EPd]PR_3$ (see the methods section). The heterobimetallic Sn−Pd bond in $[SnPd]PPh_3$ possesses a main contribution from the p orbital of Sn and a small contribution from the s orbital of Pd (Figure 3 and Table 2). Similar features are

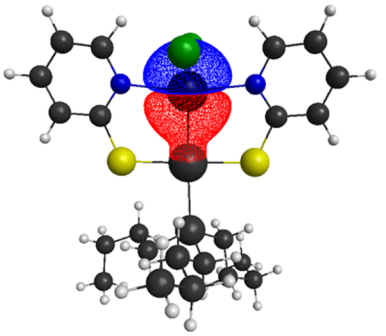

Figure 3. LMO analysis for the Sn−Pd bond in $[SnPd]PBu_3$ (contour value = 0.0008) (additional examples are given in the Supporting Information).

observed for the heterobimetallic E−Pd bond across different [SnPd] complexes containing a variety of PR_3 ligands (R = OPh, Ph, and Bu), as well as in $[GePd]PPh_3$ (see Table 2 and Supporting Information). Interestingly, $[GePd]PPh_3$ shows a small p-orbital contribution from Pd to Ge−Pd bonding. Based on these results, we conclude that the E atom (Ge or Sn) in the heteropincer ligands acts as an L-type ligand toward Pd.

Table 2. LMO Analysis: Calculated Orbital Vectors and Bonding Contributions[a]

complex/LMO	orbital vector (coefficient)	Pd bonding contribution[b]
$[GePd]PPh_3$	0.006, (s, Pd)	0.57 (s, Pd)
	0.024 (p, Pd)	2.26 (p, Pd)
	1.061 (s, Ge)	
$[SnPd]P(OPh)_3$	0.005 (s, Pd)	0.46 (s, Pd)
	1.081 (p, Sn)	
$[SnPd]PPh_3$	0.005 (s, Pd)	0.44 (s, Pd)
	1.144 (p, Sn)	
$[SnPd]PBu_3$	0.005 (s, Pd)	0.50 (s, Pd)
	0.991 (p, Sn)	

[a]See the methods section and Supporting Information [b]Ratio × 100.

Based on the exact orbital contributions, the L-type character is only slightly smaller—and the X-type character slightly higher—for Ge compared to Sn (Table 2). These observations are generally consistent with prior natural bonding orbital (NBO) analysis of similar heterobimetallic complexes.[22]

Correlating Calculations with Experiments: NMR Spectroscopy. The ^{31}P chemical shift [δ/parts per million (ppm)] of the PR_3 ligand when bound to a $[SnPd]PR_3$ pincer complex shifts upfield—to lower values—as the M−P binding enthalpy increases (ΔH); it decreases from 128.0 ppm for R = OPh, to 24.9 ppm for R = Ph, and 6.85 ppm for R = Bu. Similarly, the change in the ^{31}P chemical shift (δ/ppm) between [SnPd]-bound and free PR_3 ligand increases with the M−P binding enthalpy (ΔH); this difference goes from being almost negligible at −0.1 ppm for R = OPh, to much larger, 30.4 ppm for R = Ph, and 38.2 ppm for R = Bu (Figure 4 and Supporting Information). In other words, the weaker the Pd−P bond is, the more the PR_3 ligand in the complex appears to behave as if it was free (unbound). Relevant correlations with Tolman cone angles were reported in other systems.[40]

The Pd−P bond length is slightly longer when E = Sn than when E = Ge, a trend that seems to correlate with the bond

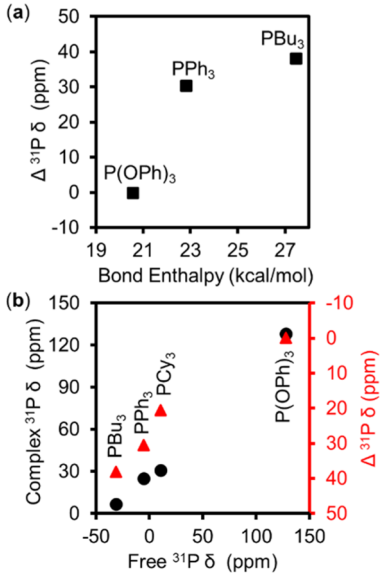

Figure 4. (a) ^{31}P NMR chemical shift difference between $[SnPd]PR_3$ complexes and free PR_3 ligand (Δ) vs calculated Pd−P bond enthalpy (ΔH). (b) Relationship between ^{31}P NMR shift of free PR_3 ligands, $[SnPd]PR_3$ complexes, and Δ (see above).

https://doi.org/10.1021/acs.inorgchem.2c00229
Inorg. Chem. 2022, 61, 6888−6897

energetics calculations as the PR_3 ligands bind more strongly to the heterobimetallic [GePd] cores. However, we observe a general lack of correlation between M−P bond length and PR_3 ligand binding affinity (ΔH or ΔG) for either germanium or tin. In the [GePd]PR_3 and [SnPd]PR_3 complexes, the Pd−P bond length increases in the order R = $P(OPh)_3$ < PBu_3 < PPh_3 (see the Supporting Information).

To further probe the bonding in these complexes, we used ^{31}P and ^{195}Pt solid-state NMR spectroscopy (ssNMR). ^{195}Pt is an abundant (33.8%) spin-1/2 nucleus. The ^{195}Pt isotropic chemical shift range and chemical shift anisotropy can be on the order of several thousand ppm.[41−43] Hence, ^{195}Pt NMR spectroscopy is a highly sensitive probe of the chemical environment. By looking at the ^{195}Pt chemical shift, $^{195}Pt-^{31}P$ ^1J-coupling, and $^{195}Pt-^{119/117}Sn$ ^1J-coupling for [SnPt]PPh_3, we can assess the chemical environment in these complexes.

Rotor-synchronized $^{31}P\{^{195}Pt\}$ J-HMQC (scalar heteronuclear multiple quantum correlation experiment) was used to analyze and determine a ^{195}Pt isotropic chemical shift of −5293 ppm for [SnPt]PPh_3 (Figure 5, see the methods section). This ^{195}Pt chemical shift is in agreement with the literature values for complexes with similar Pt environments.[25,36,44−48] We also observe a ^{31}P-^{195}Pt ^1J coupling constant of 3.3 kHz and a $^{31}P-^{119/117}Sn$ ^2J coupling constant of ca. 4.0 kHz, which correlate well with literature J-coupling values.[49,50] The ^{31}P spectrum of [GePt]PPh_3 shows a

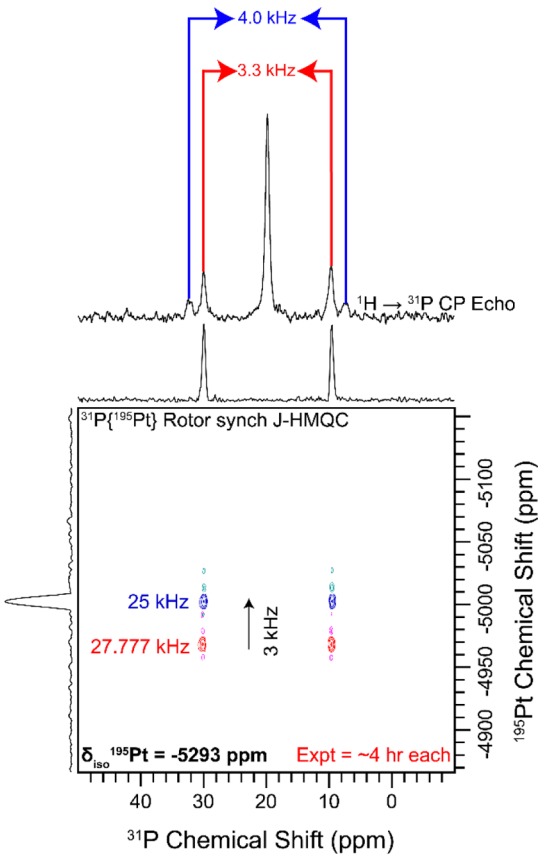

Figure 5. (Top) 1D $^1H \rightarrow ^{31}P$ CPMAS spectrum showing satellites arising from J-coupling to ^{195}Pt and ^{119}Sn (25 kHz MAS frequency). (Lower) 2D rotor-synchronized $^{31}P\{^{195}Pt\}$ J-HMQC spectra of [SnPt]PPh_3 (27.777 kHz MAS frequency). An isotropic ^{195}Pt chemical shift of −5293 ppm was determined based on the shift of the peak position with the change in MAS frequency.

$^{31}P-^{195}Pt$ ^1J constant of 2.9 kHz (see the Supporting Information), which is very similar to that of the Sn analogue.[22] A wideline ^{195}Pt MAS NMR spectrum was also recorded using a constant-time J-HMQC pulse sequence that allows for arbitrary indirect dimension spectral widths (see the Supporting Information).[51] A fit of the ^{195}Pt NMR spectrum reveals that the span (Ω) of the ^{195}Pt chemical shift tensor is 1640 ppm and that the chemical shift (CS) tensor lacks axial symmetry (skew, κ = 0). Both of these observations are somewhat surprising for a square planar Pt compound as they often possess axially symmetric CS tensors with spans in the range of 2000−10,000 ppm.[41,52,53] The low span likely arises because sulfide and phosphine are strong field ligands that form highly covalent bonds to Pt, resulting in sizeable HOMO−LUMO gaps and minimal paramagnetic deshielding.[54] The lack of axial CS tensor symmetry likely reflects the fact that the strength of covalent bonding interactions differs for the phosphine and sulfide ligands.

Ligand Exchange Experiments. To probe the PR_3 ligand binding affinities experimentally, we monitored solution phase, ligand exchange experiments by solution ^{31}P NMR spectroscopy. In each experiment, a starting complex [EPd]PR_3 was mixed with one equivalent of a different phosphorous-based ligand (phosphine or phosphite, PR'_3) (Scheme 2, Table 3).

Scheme 2. Phosphorous-Based Ligand Exchange Reactions Monitored by ^{31}P NMR Spectroscopy

When the new added PR'_3 ligand binds more strongly to [EPd] than the original PR_3 ligand, exchange occurs, and this is easily identifiable by ^{31}P NMR. When the new added PR'_3 ligand binds more weakly, this results in the same original ^{31}P NMR spectrum.

Interestingly, we find that the square planar d^8 heterobimetallic complexes readily exchange phosphorous-based ligands. An example is shown in Figure 6. When the starting complex is [SnPd]$P(OPh)_3$, there is a broad resonance at 128 ppm attributed to $P(OPh)_3$ weakly bound to Pd. When free PPh_3 is added, the new spectrum shows a sharp resonance at 128.1 ppm, corresponding to the now released, free $P(OPh)_3$, and a broad resonance around 23.5 ppm, which is reminiscent of [SnPd]PPh_3. Also of note is the absence of a free PPh_3 resonance that occurs around −5.52 ppm, indicating that ligand exchange did occur. These results are expected based on our aforementioned calculations, which show that PPh_3 binds more strongly to [SnPd] than $P(OPh)_3$. The opposite is the case when the reverse reaction is attempted. Mixing [SnPd]-PPh_3, which shows a broad resonance at 24.9 ppm, with $P(OPh)_3$ results in the same spectrum as the forward reaction, that is, a sharp resonance at 128.1 corresponding to free $P(OPh)_3$, a broad resonance at 24.9 ppm corresponding to the starting [SnPd]PPh_3 complex, and the absence of a resonance at −5.52 ppm that could indicate any release of PPh_3.

These ligand exchange reactions are also accompanied by a visible color change. For example, the addition of one equivalent of PBu_3 to a solution of [SnPd]PPh_3 in methylene chloride results in a change in color from orange to yellow (Figure 7). These changes are associated with small but easily measurable shifts in the UV−vis absorption spectrum. A first, very intense band at approximately 300 nm (ε = 40,000−

https://doi.org/10.1021/acs.inorgchem.2c00229
Inorg. Chem. 2022, 61, 6888−6897

Table 3. Ligand Exchange Experiments Followed by Solution-Phase ^{31}P NMR (^{31}P δ/ppm)[a]

#	starting cmpd.	added PR′3	products[b]
1	[GePd]PPh_3 (21.4)	$P(OPh)_3$ (128.1)	[GePd]PPh_3 (21.4), $P(OPh)_3$ (128.2) (N.R.)
2	[GePd]PPh_3 (21.4)	PBu_3 (−31.3)	[GePd]PBu_3 (5.54), PPh_3 (−5.55)
3	[SnPd]PPh_3 (24.9, br)	$P(OPh)_3$ (128.1)	[SnPd]PPh_3 (24.9, br), $P(OPh)_3$ (128.1) (N.R.)
4	[SnPd]PPh_3 (24.9, br)	PBu_3 (−31.3)	[SnPd]PBu_3 (9.81), PPh_3 (−5.55)
5	[SnPd]$P(OPh)_3$ (128, br)	PPh_3 (−5.52)	[SnPd]PPh_3 (23.5, br), $P(OPh)_3$ (128.1)
6	[SnPd]$P(OPh)_3$ (128, br)	PBu_3 (−31.3)	[SnPd]PBu_3 (8.81), $P(OPh)_3$ (128.1)
7	[SnPd]PBu_3 (6.85)	PPh_3 (−5.52)	[SnPd]PBu_3 (6.86), PPh_3 (−5.55) (N.R.)
8	[SnPd]PBu_3 (6.85)	$P(OPh)_3$ (128.1)	[SnPd]PBu_3 (6.86), $P(OPh)_3$ (128.1) (N.R.)

[a]See the methods section. [b]N.R. = no reaction.

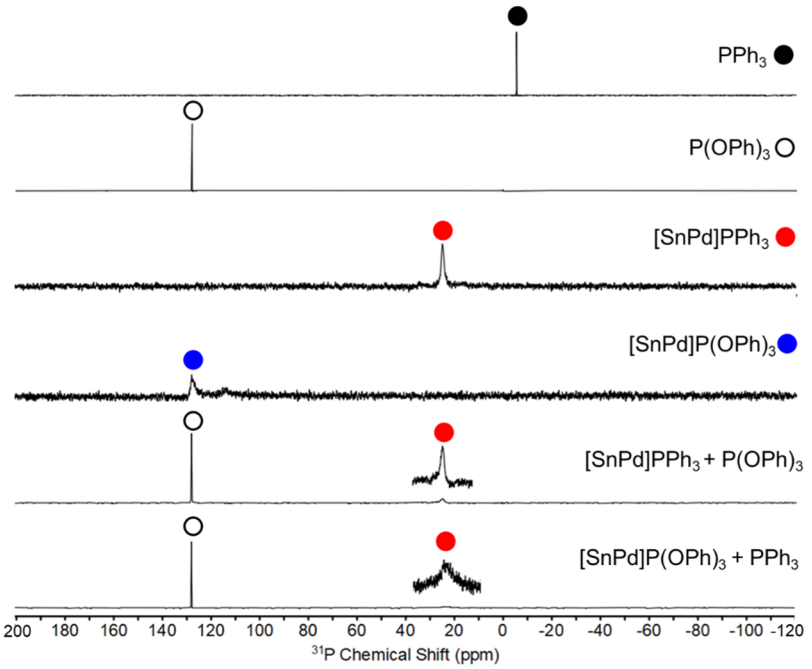

Figure 6. Ligand exchange reaction between [SnPd]PPh_3 and $P(OPh)_3$ (see also the Supporting Information).

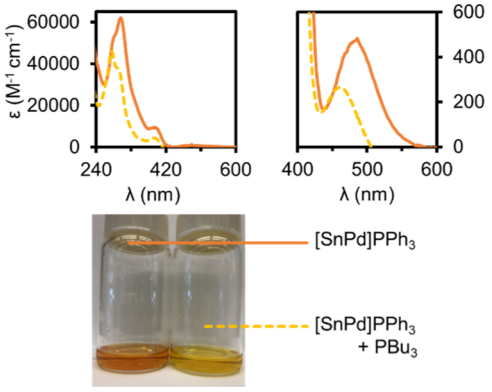

Figure 7. UV−vis absorption spectra and optical image of [SnPd]PPh_3 in CH_2Cl_2 before and after the addition of one equivalent of PBu_3.

60,000 M^{-1} cm^{-1}) may be assigned as a charge-transfer band. Replacing PPh_3 with the more electron-donating PBu_3 blue shifts the band maximum slightly, from 302 to 299 nm. Future studies including time-dependent DFT or similar methods will be required to specifically assign these bands as either LM- or ML-CT transitions. A less intense visible band (ε = 200−400 M^{-1} cm^{-1}) also blue shifts from 488 to 465 nm. This may be assigned to a Laporte-allowed d−d transition as these complexes lack centrosymmetry.[55]

Heterobimetallic 10−14 Complexes as Catalysts. Pincer complexes are of great interest as catalysts for cross-coupling reactions as the pincer ligand can help enhance the reactivity and selectivity of the transition metal. Here, we specifically find that heterobimetallic bis(pyridine-2-thiolato)-dichloro-germanium and tin complexes of palladium(II) are active catalysts in the Negishi cross-coupling reaction between ethyl-*o*-iodobenzoate (**1**) and cyclohexyl zinc chloride (**2**) (Scheme 3). In the presence of the [EPd] pincer catalysts, full conversion to ethyl 2-cyclohexylbenzoate (red **3**) is achieved within 20 min at room temperature (25 °C), with only small

Scheme 3. Negishi Coupling of Ethyl-*o*-iodobenzoate (**1**) and Cyclohexyl Zinc Chloride (**2**)

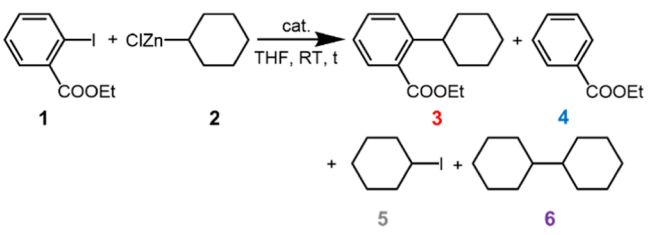

https://doi.org/10.1021/acs.inorgchem.2c00229
Inorg. Chem. 2022, 61, 6888−6897

amounts of byproducts ethylbenzoate (blue **4**), iodocyclohexane (gray **5**), and bicyclohexyl (violet **6**). This is comparable to the results obtained when the catalyst is a monometallic SNS complex of Pd[56,57] and significantly better than those obtained with commercially available $Pd(PPh_3)_4$ (Figure 8 and Table 4).

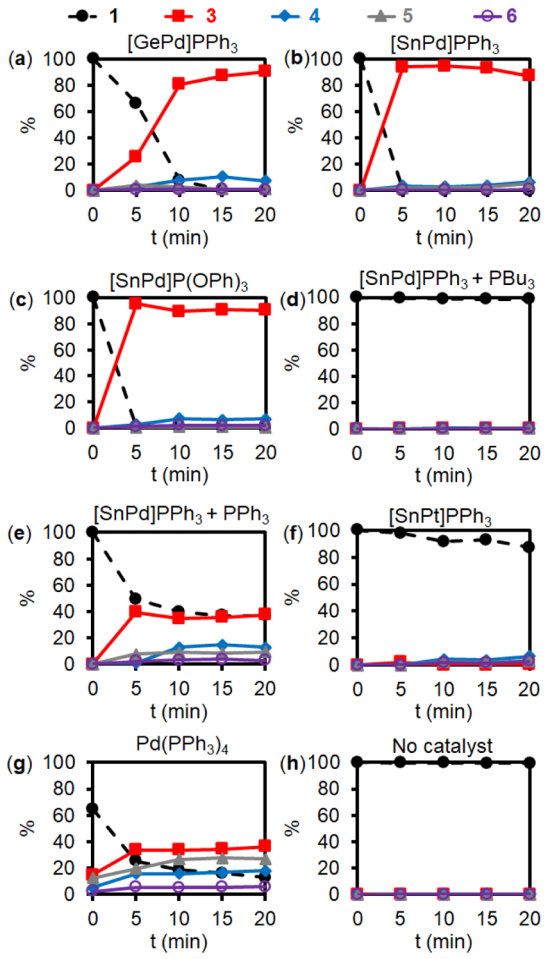

Figure 8. Negishi coupling between ethyl-2-iodobenzoate (**1**) and cyclohexylzinc chloride (**2**) —see Scheme 3—catalyzed by (a) $[GePd]PPh_3$, (b) $[SnPd]PPh_3$, (c) $[SnPd]P(OPh)_3$, (d) $[SnPd]PPh_3$ + 1 equiv. PBu_3, (e) $[SnPd]PPh_3$ + 1 equiv PPh_3, (f) $[SnPt]PPh_3$, (g) $Pd(PPh_3)_4$, and (h) no catalyst (see the methods section).

To examine the effects of the heterobimetallic complex structure and composition on catalytic properties, we compared the complexes $[GePd]PPh_3$ and $[SnPd]PPh_3$, which only differ in group 14 element. When $[GePd]PPh_3$ is used as the catalyst, the Negishi reaction is completed after 15 min, with the coupling target (**3**) being the major product (90%) (Figure 8a and Table 4). Furthermore, only 8% of the dehalogenated side product (**4**) and minimal amounts of (**5**) and (**6**) are present (see Scheme 3). Notably, the reaction proceeds more quickly with $[SnPd]PPh_3$, reaching completion in as little as 5 min (Figure 8b and Table 4). Because PPh_3 binds more weakly to Pd in the more active $[SnPd]PPh_3$ complex, this suggests that the catalyst becomes more readily available when PR_3 ligand dissociation is easier, perhaps due to the opening of an active coordination site at the metal.

To further probe the effect of PR_3 ligand-binding affinity on the catalytic activity of the heterobimetallic complexes, we tested the $[SnPd]PBu_3$ complex as a catalyst. Because PBu_3 binds stronger to Pd than PPh_3—as evidenced by our aforementioned calculations and ligand exchange experiments—we hypothesized that in this case, the catalytic reaction should proceed more slowly. To test this idea, we generated the $[SnPd]PBu_3$ complex in situ through the addition of one equivalent of PBu_3 to $[SnPd]PPh_3$ (note: To date, $[SnPd]PBu_3$ has been difficult to isolate as crystals,[36] hence the advantage of generating it through this method). As expected, the in situ generated $[SnPd]PBu_3$ displays minimal activity, with less than 2% conversion after 20 min (Figure 8d and Table 4). This shows that the reaction is severely inhibited by the presence of the strongly binding PBu_3 ligand. Because the presence of the displaced PPh_3 in the reaction solution could also hinder catalysis, we repeated the reaction with a mixture of $[SnPd]PPh_3$ and one added equivalent of PPh_3. In the presence of the excess PPh_3, only a fraction of the original conversion, 63.1%, is observed after 20 min, with a lower selectivity for the coupling product (60%) (Figure 8e and Table 4). Therefore, while excess PPh_3 can also hinder access to the active site, it is the more strongly binding PBu_3 that most significantly inhibits the catalyst performance, supporting our hypothesis.

Finally, we looked at the effect of the transition metal on the catalyst performance by testing $[SnPt]PPh_3$ in the coupling reaction. When Pt is used instead of Pd, the reaction displays drastically different behavior. Only 12.7% conversion and 4% selectivity to the coupling product (**3**) are achieved after 20 min. The major product is the dehalogenated compound (**4**) (Scheme 3). Because our calculations suggest that PR_3 ligand binding is much weaker for Pt than that for Pd, this lack of activity cannot be attributed to being able to access a coordination site at the metal. Instead, this is consistent with C−C coupling reactions occurring much more easily in Pd than that in Pt complexes because the Pd−R bonds are weaker—and easier to cycle through—than the analogous Pt−R bonds.[58,59]

Overall, like their monometallic analogues,[56,57] heterobimetallic 10−14 E−M complexes are active catalysts in Negishi cross coupling reactions. Unlike the monometallic versions, however, the reactivity of the heterobimetallic complexes can also be tuned by changing the group 14 element, in addition to the transition metal, and the phosphine ligand. Furthermore,

Table 4. Negishi Coupling of Ethyl-*o*-iodobenzoate (1) and Cyclohexyl Zinc Chloride (2) Catalyzed by Heterobimetallic Complexes (See Scheme 3)[a]

Catalyst	Conv.[b] (%)	TON[c] (TOF, h^{-1})	Selectivity[b] 3	4	5	6
None	0.434	-	0	56	26	18
$[GePd]PPh_3$	100	200 (600)	90	8	1	1
$[SnPd]PPh_3$	100	200 (600)	87	7	5	1
$[SnPd]P(OPh)_3$	99.5	199 (597)	90	7	1	2
$[SnPd]PPh_3$ + PBu_3 (1 equiv)	1.56	3.12 (9.36)	37	32	26	5
$[SnPd]PPh_3$ + PPh_3 (1 equiv)	63.1	126 (378)	60	20	15	5
$[SnPt]PPh_3$	12.7	25.4 (76.2)	4	51	25	20
$Pd(PPh_3)_4$	87.1	174 (523)	42	21	31	7

[a]Reaction conditions: 0.005 mmol catalyst (0.5 mol %), 1 mmol (**1**), 2 mmol (**2**), in 4 mL THF, 25 °C, 20 min (see the methods section). [b]Determined by GC−MS using naphthalene as an internal standard. [c]TON = moles of (**1**) consumed/moles of catalyst; TOF = TON/time.

https://doi.org/10.1021/acs.inorgchem.2c00229
Inorg. Chem. 2022, 61, 6888−6897

future studies will be directed at exploring what effect the E−Cl bonds may have during the catalytic cycle. This feature is unique to the heteropincer ligand backbone and is expected to offer unique reactivity: For example, activation of related Si−F bonds was recently used to develop an unprecedented Sila-Negishi cross-coupling reaction.[60]

CONCLUSIONS

In summary, we have examined the binding affinity of phosphorous-based ligands to heterobimetallic 10−14 complexes both theoretically and experimentally. First, using two different computational methods, we calculated the BDEs and enthalpies for these complexes and observed that the M−P binding affinity decreases in the order PBu_3 > PPh_3 > $P(OPh)_3$ for both Ge- and Sn-based complexes. Experimentally, using a series of ^{31}P solution NMR exchange reactions, we observe the same order of binding affinities. Additionally, we found that the change in the ^{31}P NMR chemical shifts between the [SnPd]PR_3 complexes and the free PR_3 ligands correlates to the binding strength between the ligands and the heterobimetallic [EM] core.

To further determine the utility of heterobimetallic 10−14 complexes, we demonstrated the [EPd]PR_3 complexes as active catalysts for the Negishi coupling between ethyl-2-iodobenzoate and cyclohexyl zinc chloride. Our findings show that the group 14 or "tetrel" element, the exact phosphine ligand, and the transition metal all play determinant roles on the catalytic activity: tin complexes are a more active than germanium ones, palladium complexes are active, whereas platinum complexes are not, and the more strongly the phosphine ligand binds to the [EM] core, the less active the catalyst is. We believe that these findings will aid in future studies aimed at designing and optimizing the heterobimetallic pincer complexes for different applications.

METHODS

Materials. Triphenylphosphine (PPh_3, 99%), triphenylphosphite ($P(OPh)_3$, 97%), tri-*n*-butylphosphine (PBu_3, 99%), zinc chloride ($ZnCl_2$, anhydrous, 97%), and tetrakis(triphenylphosphine)palladium [$Pd(PPh_3)_4$, 99%] were purchased from Strem. Cyclohexylmagnesium chloride (1 M in MeTHF) and ethyl *o*-iodobenzoate (98%) were purchased from Alfa Aesar. Methylene dichloride-d_2 (CD_2Cl_2) was purchased from Cambridge Isotope Laboratories, degassed, and dried over activated molecular sieves. Tetrahydrofuran (THF, inhibitor-free, >99.9%) was dried and deoxygenated using an IT PureSolv system. The heterobimetallic pincer complexes [GePd]PPh_3, [SnPd]PPh_3, [SnPd]$P(OPh)_3$, [SnPd]PBu_3, and [SnPt]PPh_3 were synthesized using previously reported, available methods.[21,22,36]

Calculations. All calculations were carried out using GAMESS (2014 R1).[61,62] The calculations at the DFT level of theory were carried out using the B3LYP functional[63−65] with the Stevens/Basch/Krauss/Jasien/Cundari (SBKJC) basis set with effective core potentials for Pd, Pt, Sn, and Ge[66] and the 6-31G(d,p) basis set for all other elements.[67−70] RHF calculations (ran without DFT) used the MIDI basis set for all elements.[71] The calculations carried out as a lower level of theory provided similar results to those with DFT and were less computationally expensive. The starting geometry for each structural optimization was taken from single-crystal data available in the Cambridge Structural Database (CSD)[72] where applicable. Hessian calculations were performed to verify that each optimized geometry had no imaginary vibrational frequencies. The thermodynamic parameters ΔH and ΔG and zero-point energy corrections were calculated at 298.15 K and 1 atm. Results were visualized using MacMolPlt.[73] LMO analysis was carried out with GAMESS by RHF/MIDI and the Edmiston and Ruedenberg method.[74,75]

NMR Spectroscopy. Exchange experiments in solution were performed on a Bruker Avance III 600 spectrometer at room temperature. ^{31}P NMR shifts (243.04 MHz) are given in ppm and referenced to the ^1H spectrum (600.39 MHz) residual solvent peaks using indirect referencing methods.[76] For each exchange reaction, approximately 0.02 mmol of the starting complex [EPd]PR_3 was dissolved in 0.5 mL of CD_2Cl_2, followed by an initial spectrum collection. Next, 1 equiv (0.02 mmol) of a different phosphorous-based ligand, PR'_3, was added directly to the NMR tube and mixed well before obtaining the new spectrum. In the cases where PBu_3 was the added ligand, the ligand exchange process was carried out in a glovebox, and a J Young tube was used.

Solid-state NMR experiments were performed on a 9.4 T ($\nu_0(^1H)$ = 400 MHz) Bruker wide-bore magnet spectrometer equipped with a Bruker Avance III HD console. Experiments were performed with a Bruker 2.5 mm HXY magic-angle spinning (MAS) probe in the triple resonance mode. All samples were packed into 2.5 mm zirconia rotors in air. N_2 gas was used to spin the rotor for MAS experiments. Before the NMR experiments, the magic angle was precisely set by narrowing the second-order spinning sideband peak width of potassium bromide. The ^1H RF powers were calibrated directly on each sample using a $\pi/2$-spin-lock pulse sequence to determine the second-order rotary resonance recoupling condition ($\nu_1 = 2 \times \nu_{rot}$). A 100 kHz RF field was used for all ^1H pulses. Most experiments were performed with a 25 kHz MAS frequency, with a second MAS frequency of 27.777 kHz used for some J-HMQC experiments. ^1H longitudinal relaxation (T_1) measurements were performed on each sample using a saturation recovery experiment. All experiments were recorded with longitudinal relaxation delays of 1.3 × T_1 corresponding to delays of 42.9 s for [SnPt]PPh_3 and 32.5 s for [GePt]PPh_3. Cross-polarization (CP) was directly optimized on each sample by monitoring the signal intensity of a $^1H \rightarrow {}^{31}P$ CPMAS spectrum while varying the ^1H spin-lock RF fields and holding the ^{31}P spin-lock RF field constant. $^1H-{}^{31}P$ CP echo experiments used 16 scans with an echo delay of one rotor cycle. The $^{31}P\{^{195}Pt\}$ J-HMQC experiments used eight scans with a 160 or 144 μs *J*-evolution time (half-echo duration) that approximately corresponds to the optimal duration for $^{31}P-{}^{195}Pt$ ^1J values of ca. 3200 Hz. The rotor-synchronized J-HMQC spectra were obtained with 40 and 44 hyper-complex indirect dimension points for 25 and 27.777 kHz MAS, respectively. ^1H chemical shifts were referenced to a 1% solution of tetramethylsilane in $CDCl_3$ (δ_{iso} = 0 ppm) with a secondary standard of solid adamantane (δ_{iso} = 1.76 ppm). ^{195}Pt chemical shifts were indirectly referenced to a 1.2 M solution of Na_2PtCl_6 in D_2O (δ_{iso} = 0 ppm) using the IUPAC recommended Larmor frequency ratio of 21.496784% for ^{195}Pt as compared to ^1H.[76] ^{31}P chemical shifts were indirectly referenced to a 85% solution of H_3PO_4 in H_2O (δ_{iso} = 0 ppm) using the IUPAC recommended Larmor frequency ratio of 40.480742% for ^{31}P as compared to ^1H.[76] All NMR spectra were processed in Bruker Topspin 3.6.2.

UV−Vis Spectroscopy. UV−vis absorbance spectra were measured on a photodiode array Agilent 8453 spectrophotometer with solvent (dichloromethane) subtracted from all spectra.

Negishi Coupling Reactions. Catalysis experiments were run following similar procedures in the literature.[56,57] For each reaction, 2 mmol of $ZnCl_2$ was dissolved in 1 mL of dry THF in a small round-bottom flask in a glovebox. The flask was then taken out and attached to a Schlenk line, where it was evacuated and flushed with Ar. Next, 2 mL of cyclohexylmagnesium chloride (1 M in MeTHF) was added to the flask dropwise, and the solution was allowed to stir for 1 h at RT. Approximately 0.005 mmol of the catalyst was dissolved in 1 mL of THF and injected into the reaction flask, followed by 1 mmol (~0.1 mL) of ethyl *o*-iodobenzoate. The reaction was allowed to proceed for 20 min, with small aliquots taken at 5 min intervals and prepared for analysis by GCMS. GCMS analysis was performed on an Agilent 7250 GC QTOF instrument using naphthalene as an internal standard.

https://doi.org/10.1021/acs.inorgchem.2c00229
Inorg. Chem. 2022, 61, 6888−6897

■ ASSOCIATED CONTENT

Supporting Information

The Supporting Information is available free of charge at https://pubs.acs.org/doi/10.1021/acs.inorgchem.2c00229.

Additional calculations, including bond lengths, HOMO/LUMO diagrams, LMO analyses, ^{31}P NMR and bond enthalpy data, and exchange experiments (PDF)

■ AUTHOR INFORMATION

Corresponding Author

Javier Vela − *Department of Chemistry, Iowa State University, Ames, Iowa 50011, United States; US DOE Ames Laboratory, Ames, Iowa 50011, United States;* orcid.org/0000-0001-5124-6893; Email: vela@iastate.edu

Authors

Carena L. Daniels − *Department of Chemistry, Iowa State University, Ames, Iowa 50011, United States*

Eunbyeol Gi − *Department of Chemistry, Iowa State University, Ames, Iowa 50011, United States; US DOE Ames Laboratory, Ames, Iowa 50011, United States*

Benjamin A. Atterberry − *Department of Chemistry, Iowa State University, Ames, Iowa 50011, United States; US DOE Ames Laboratory, Ames, Iowa 50011, United States*

Rafael Blome-Fernández − *Department of Chemistry, Iowa State University, Ames, Iowa 50011, United States*

Aaron J. Rossini − *Department of Chemistry, Iowa State University, Ames, Iowa 50011, United States; US DOE Ames Laboratory, Ames, Iowa 50011, United States;* orcid.org/0000-0002-1679-9203

Complete contact information is available at: https://pubs.acs.org/10.1021/acs.inorgchem.2c00229

Author Contributions

⊥C.L.D. and E.G. contributed equally.

Notes

The authors declare no competing financial interest.

■ ACKNOWLEDGMENTS

Synthesis, calculations, and catalyst testing were made possible by a grant from the U.S. National Science Foundation, Division of Chemistry, Macromolecular, Supramolecular, and Nanochemistry Program (1905066) to J.V. B.A.A. and A.J.R. thank the U.S. Department of Energy (DOE), Office of Science, Basic Energy Sciences, Materials Science and Engineering Division for supporting the solid-state NMR studies. The Ames Laboratory is operated for the U.S. DOE by Iowa State University under contract DE-AC02-07CH11358. A.J.R. acknowledges the additional support from the Alfred P. Sloan Foundation through a Sloan research fellowship. We thank Mark Gordon, Yu Lim Kim, Levi Stanley, Huajun Fan, and Megan Knobeloch for useful discussions.

■ REFERENCES

(1) González-Sebastián, L.; Morales-Morales, D. Cross-coupling Reactions Catalysed by Palladium Pincer complexes. A Review of Recent Advances. *J. Organomet. Chem.* **2019**, *893*, 39−51.

(2) Selander, N.; Szabó, K. J. Catalysis by Palladium Pincer Complexes. *Chem. Rev.* **2011**, *111*, 2048−2076.

(3) Albrecht, M.; Van Koten, G. Platinum Group Organometallics Based on "Pincer" Complexes: Sensors, Switches, and Catalysts. *Angew. Chem., Int. Ed.* **2001**, *40*, 3750−3781.

(4) Flores-Rojas, G.; González-Sebastián, L.; Reyes-Martínez, R.; Aguilar-Castillo, B. A.; Hernández-Ortega, S.; Morales-Morales, D. Synthesis and Characterization of Pd(II) Complexes Bearing NS, CS, SNS and SCS ligands. Evaluation of their Microwave Assisted Catalytic Activity in C−C Coupling Reactions. *Polyhedron* **2020**, *185*, 114601.

(5) Basauri-Molina, M.; Hernández-Ortega, S.; Morales-Morales, D. Microwave-Assisted C−C and C−S Couplings Catalysed by Organometallic Pd-SCS or Coordination Ni-SNS Pincer Complexes. *Eur. J. Inorg. Chem.* **2014**, *27*, 4619−4625.

(6) Tyson, G. E.; Tokmic, K.; Oian, C. S.; Rabinovich, D.; Valle, H. U.; Hollis, T. K.; Kelly, J. T.; Cuellar, K. A.; McNamara, L. E.; Hammer, N. I.; Webster, C. E.; Oliver, A. G.; Zhang, M. Synthesis, Characterization, Photophysical Properties, and Catalytic Activity of an SCS bis(N-Heterocyclic Thione) (SCS-NHT) Pd Pincer Complex. *Dalton Trans.* **2015**, *44*, 14475−14482.

(7) Graziano, B. J.; Vollmer, M. V.; Lu, C. C. Cooperative Bond Activation and Facile Intramolecular Aryl Transfer of Nickel−Aluminum Pincer-type Complexes. *Angew. Chem., Int. Ed.* **2021**, *60*, 15087−15094.

(8) Takaya, J.; Iwasawa, N. Structure, and Catalysis of Palladium Complexes Bearing a Group 13 Metalloligand: Remarkable Effect of an Aluminum-Metalloligand in Hydrosilylation of CO_2. *J. Am. Chem. Soc.* **2017**, *139*, 6074−6077.

(9) Takaya, J. Catalysis Using Transition Metal Complexes Featuring Main Group Metal and Metalloid Compounds as Supporting Ligands. *Chem. Sci.* **2021**, *12*, 1964−1981.

(10) Whited, M. T. Pincer-Supported Metal/Main-Group Bonds as Platforms for Cooperative Transformations. *Dalton Trans.* **2021**, *50*, 16443−16450.

(11) Cabeza, J. A.; García-Álvarez, P.; Laglera-Gándara, C. J. The Transition Metal Chemistry of PGeP and PSnP Pincer Heavier Tetrylenes. *Eur. J. Inorg. Chem.* **2020**, *2020*, 784−795.

(12) Simon, M.; Breher, F. Multidentate Silyl Ligands in Transition Metal Chemistry. *Dalton Trans.* **2017**, *46*, 7976−7997.

(13) Zhu, C.; Takaya, J.; Iwasawa, N. Use of Formate Salts as a Hydride and a CO_2 Source in PGeP-Palladium Complex-Catalyzed Hydrocarboxylation of Allenes. *Org. Lett.* **2015**, *17*, 1814−1817.

(14) Takaya, J.; Iwasawa, N. Synthesis, Structure, and Reactivity of a Mononuclear η2-(Ge−H)-palladium(0) Complex Bearing a PGeP-Pincer-Type Germyl Ligand: Reactivity Differences between Silicon and Germanium. *Eur. J. Inorg. Chem.* **2018**, *2018*, 5012−5018.

(15) Álvarez-Rodríguez, L.; Brugos, J.; Cabeza, J.; García-Álvarez, P.; Pérez-Carreño, E.; Polo, D. Synthesis and Initial Transition Metal Chemistry of the First PGeP Pincer-Type Germylene. *Chem. Commun.* **2017**, *53*, 893−896.

(16) Álvarez-Rodríguez, L.; Brugos, J.; Cabeza, J. A.; García-Álvarez, P.; Pérez-Carreño, E. From a Diphosphanegermylene to Nickel, Palladium, and Platinum Complexes Containing Germyl PGeP Pincer Ligands. *Chem.—Eur. J.* **2017**, *23*, 15107−15115.

(17) Cabeza, J. A.; Fernández, I.; Fernández-Colinas, J. M.; García-Álvarez, P.; Laglera-Gándara, C. J. A Germylene Supported by Two 2-Pyrrolylphosphane Groups as Precursor to PGeP Pincer Square-Planar Group 10 Metal(II) and T-Shaped Gold(I) Complexes. *Chem. - Eur. J.* **2019**, *25*, 12423−12430.

(18) Watanabe, T.; Kasai, Y.; Tobita, H. A Nickel Complex Containing a Pyramidalized, Ambiphilic Pincer Germylene Ligand. *Chem.—Eur. J.* **2019**, *25*, 1391−13495.

(19) Cabon, Y.; Kleijn, H.; Siegler, M. A.; Spek, A. L.; Gebbink, R. J. M. K.; Deelman, B.-J. Dichlorostannylene Complexes of Group 10 Metals, A Unique Bonding Mode Stabilized by Bridging 2-Pyridyldiphenylphosphine Ligands. *Dalton Trans.* **2010**, *39*, 2423−2427.

(20) Brendler, E.; Wächtler, E.; Heine, T.; Zhechkov, L.; Langer, T.; Pöttgen, R.; Hill, A. F.; Wagler, J. Stannylene or Metallastanna(IV)-

ocane: A Matter of Formalism. *Angew. Chem., Int. Ed.* **2011**, *50*, 4696−4700.
(21) Wächtler, E.; Gericke, R.; Zhechkov, L.; Heine, T.; Langer, T.; Gerke, B.; Pöttgen, R.; Wagler, J. Pyridine-2-Thiolate Bridged Tin−Palladium Complexes with $Sn(PdN_2Cl_2)$, $Sn(PdN_2S_2)$, $Sn(PdN_2C_2)$ and $Sn(Pd_2N_4)$ Skeletons. *Chem. Commun.* **2014**, *50*, 5382−5384.
(22) Wächtler, E.; Gericke, R.; Brendler, E.; Gerke, B.; Langer, T.; Pöttgen, R.; Zhechkov, L.; Heine, T.; Wagler, J. Group 10−Group 14 Metal Complexes $[E{-}TM]^{IV}$: The Role of the Group 14 Site as an L, X and Z-Type Ligand. *Dalton Trans.* **2016**, *45*, 14252−14264.
(23) Wächtler, E.; Wahlicht, S.; Privér, S. H.; Bennett, M. A.; Gerke, B.; Pöttgen, R.; Brendler, E.; Gericke, R.; Wagler, J.; Bhargava, S. K. Tin(IV) Compounds with 2-$C_6F_4PPh_2$ Substituents and Their Reactivity toward Palladium(0): Formation of Tin−Palladium Complexes via Oxidative Addition. *Inorg. Chem.* **2017**, *56*, 5316−5327.
(24) Tayaka, J.; Nakamura, S.; Iwasawa, N. Synthesis, Structure, and Catalytic Activity of Palladium Complexes Bearing a Tridentate PXP-Pincer Ligand of Heavier Group 14 Element (X = Ge, Sn). *Chem. Lett.* **2012**, *41*, 967−969.
(25) Warsink, S.; Derrah, E. J.; Boon, C. A.; Cabon, Y.; de Pater, J. J. M.; Lutz, M.; Klein Gebbink, R. J. M.; Deelman, B.-J. Intramolecularly Stabilised Group 10 Metal Stannyl and Stannylene Complexes: Multipathway Synthesis and Observation of Platinum-to-Tin Alkyl Transfer. *Chem.—Eur. J.* **2015**, *21*, 1765−1779.
(26) Wade, C. R.; Ke, I.-S.; Gabbaï, F. P. Sensing of Aqueous Fluoride Anions by Cationic Stibine−Palladium Complexes. *Angew. Chem., Int. Ed.* **2012**, *51*, 478−481.
(27) Yang, H.; Gabbaï, F. P. Solution and Solid-State Photoreductive Elimination of Chlorine by Irradiation of a $[PtSb]^{VII}$ Complex. *J. Am. Chem. Soc.* **2014**, *136*, 10866−10869.
(28) You, D.; Gabbaï, F. P. Unmasking the Catalytic Activity of a Platinum Complex with a Lewis Acidic, Non-innocent Antimony Ligand. *J. Am. Chem. Soc.* **2017**, *139*, 6843−6846.
(29) You, D.; Yang, H.; Sen, S.; Gabbaï, F. P. Modulating the σ-Accepting Properties of an Antimony Z-type Ligand via Anion Abstraction: Remote-Controlled Reactivity of the Coordinated Platinum Atom. *J. Am. Chem. Soc.* **2018**, *140*, 9644−9651.
(30) Furan, S.; Hupf, E.; Boidol, J.; Brünig, J.; Lork, E.; Mebs, S.; Beckmann, J. Transition Metal Complexes of Antimony Centered Ligands Based Upon Acenaphthyl Scaffolds. Coordination Non-innocent or Not? *Dalton Trans.* **2019**, *48*, 4504−4513.
(31) You, D.; Smith, J. E.; Sen, S.; Gabbaï, F. P. A Stiboranyl Platinum Triflate Complex as an Electrophilic Catalyst. *Organometallics* **2020**, *39*, 4169−4173.
(32) Lin, T.-P.; Ke, I.-S.; Gabbaï, F. P. σ-Accepting Properties of a Chlorobismuthine Ligand. *Angew. Chem., Int. Ed.* **2012**, *51*, 4985−4988.
(33) Tschersich, C.; Limberg, C.; Roggan, S.; Herwig, C.; Ernsting, N.; Kovalenko, S.; Mebs, S. Gold− and Platinum−Bismuth Donor−Acceptor Interactions Supported by an Ambiphilic PBiP Pincer Ligand. *Angew. Chem., Int. Ed.* **2012**, *51*, 4989−4992.
(34) Tschersich, C.; Braun, B.; Herwig, C.; Limberg, C. PBiP Pincer Complexes of Platinum, Palladium, and Iridium Featuring Metal−Metal Bonds Synthesized by Oxidative Addition of Bismuth− Halide Bonds. *Organometallics* **2015**, *34*, 3782−3787.
(35) Tschersich, C.; Hoof, S.; Frank, N.; Herwig, C.; Limberg, C. The Effect of Substituents at Lewis Acidic Bismuth(III) Centers on Its Propensity to Bind a Noble Metal Donor. *Inorg. Chem.* **2016**, *55*, 1837−1842.
(36) Daniels, C. L.; Knobeloch, M.; Yox, P.; Adamson, M. A. S.; Chen, Y.; Dorn, R. W.; Wu, H.; Zhou, G.; Fan, H.; Rossini, A. J.; Vela, J. Intermetallic Nanocatalysts from Heterobimetallic Group 10−14 Pyridine-2-Thiolate Precursors. *Organometallics* **2020**, *39*, 1092−1104.
(37) Daniels, C. L.; Mendivelso-Perez, D. L.; Rosales, B. A.; You, D.; Sahu, S.; Jones, J. S.; Smith, E. A.; Gabbaï, F. P.; Vela, J. Heterobimetallic Single-Source Precursors: A Springboard to the Synthesis of Binary Intermetallics. *ACS Omega* **2019**, *4*, 5197−5203.
(38) Daniels, C. L.; Liu, D.-J.; Adamson, M. A. S.; Knobeloch, M.; Vela, J. Azo(xy) vs Aniline Selectivity in Catalytic Nitroarene Reduction by Intermetallics: Experiments and Simulations. *J. Phys. Chem. C* **2021**, *125*, 24440−24450.
(39) Huggett, P. G.; Manning, K.; Wade, K. The Relative Lewis Acidities of Silicon Tetrachloride, Germanium Tetrachloride and Tin Tetrachloride Towards Acetonitrile, Acrylonitrile, Ethyl Acetate, Diethyl Ether and Tetrahydrofuran; Vapour Pressure-composition Studies. *J. Inorg. Nucl. Chem.* **1980**, *42*, 665−673.
(40) Hunter, A. D.; Williams, T. R.; Zarzyczny, B. M.; Bottesch, H. W.; Dolan, S. A.; McDowell, K. A.; Thomas, D. N.; Mahler, C. H.; II. Correlations among ^{31}P NMR Coordination Chemical Shifts, Ru−P Bond Distances, and Enthalpies of Reaction in $Cp'Ru(PR_3)_2Cl$ Complexes (Cp' = η^5-C_5H_5, η^5-C_5Me_5; PR_3 = PMe_3, $PPhMe_2$, PPh_2Me, PPh_3, PEt_3, P^nBu_3). *Organometallics* **2016**, *35*, 2701−2706.
(41) Lucier, B. E. G.; Johnston, K. E.; Xu, W.; Hanson, J. C.; Senanayake, S. D.; Yao, S.; Bourassa, M. W.; Srebro, M.; Autschbach, J.; Schurko, R. W. Unravelling the Structure of Magnus' Pink Salt. *J. Am. Chem. Soc.* **2014**, *136*, 1333−1351.
(42) Schurko, R. W. Ultra-Wideline Solid-State NMR Spectroscopy. *Acc. Chem. Res.* **2013**, *46*, 1985−1995.
(43) MacGregor, A. W.; O'Dell, L. A.; Schurko, R. W. New Methods for the Acquisition of Ultra-Wideline Solid-State NMR Spectra of Spin-1/2 Nuclides. *J. Magn. Reson.* **2011**, *208*, 103−113.
(44) Klein, A.; Schurr, T.; Knödler, A.; Gudat, D.; Klinkhammer, K.-W.; Jain, V. K.; Záliš, S.; Kaim, W. Multiple Isomerism (cis/trans; syn/anti) in $[(dmso)_2Pt(aryl)_2]$ Complexes: A Combined Structural, Spectroscopic, and Theoretical Investigation. *Organometallics* **2005**, *24*, 4125−4131.
(45) Knödler, A.; Kaim, W.; Jain, V. K.; Záliš, S. Dimethylplatinum-(II) and Tetramethylplatinum(IV) Complexes of 1-Methyl-(2-Alkylthiomethyl)-1H-Benzimidazoles: Experimental and DFT-Calculated Structures and NMR spectra. *J. Organomet. Chem.* **2002**, *655*, 218−226.
(46) De Castro, V. D.; Filgueiras, C. A. L.; de Lima, G. M.; Gambardella, M. T. P.; Speziali, N. L. Reactivity of [SnPh3(η^1-2-PyS)] Towards Pt and Ni Complexes. *Main Group Met. Chem.* **2001**, *24*, 761−764.
(47) Hope, E. G.; Levason, W.; Powell, N. A. Coordination Chemistry of Higher Oxidation States. Part 21. Platinum-195 NMR Studies of Platinum(II) and Platinum(IV) Complexes of Bi- and Multi-dentate Phosphorus, Arsenic and Sulphur Ligands. *Inorg. Chim. Acta* **1986**, *115*, 187−192.
(48) Nelson, J. H.; Cooper, V.; Rudolph, R. W. The Nature of Pt/$SnCl_3^-$ Salts in Solution by Multinuclear NMR. Unusually Large Spin-Spin Coupling, Cluster Size, Fluxionality, and a Caveat. *Inorg. Nucl. Chem. Lett.* **1980**, *16*, 263−265.
(49) Pidcock, A.; Richards, R. E.; Venanzi, L. M. $^{195}Pt{-}^{31}P$ Nuclear Spin Coupling Constants and the Nature of the Trans-Effect in Platinum Complexes. *J. Chem. Soc. A* **1966**, 1707−1710.
(50) Arras, J.; Eichele, K.; Maryasin, B.; Schubert, H.; Ochsenfeld, C.; Wesemann, L. Intermolecular $^{119}Sn,^{31}P$ Through-Space Spin−Spin Coupling in a Solid Bivalent Tin Phosphido Complex. *Inorg. Chem.* **2016**, *55*, 4669−4675.
(51) Rossini, A. J.; Hanrahan, M. P.; Thuo, M. Rapid Acquisition of Wideline MAS Solid-State NMR Spectra with Fast MAS, Proton Detection, and Dipolar HMQC Pulse Sequences. *Phys. Chem. Chem. Phys.* **2016**, *18*, 25284−25295.
(52) Lucier, B. E. G.; Reidel, A. R.; Schurko, R. W. Multinuclear Solid-State NMR of Square-Planar Platinum Complexes — Cisplatin and Related Systems. *Can. J. Chem.* **2011**, *89*, 919−937.
(53) Venkatesh, A.; Lund, A.; Rochlitz, L.; Jabbour, R.; Gordon, C. P.; Menzildjian, G.; Viger-Gravel, J.; Berruyer, P.; Gajan, D.; Copéret, C.; Lesage, A.; Rossini, A. J. The Structure of Molecular and Surface Platinum Sites Determined by DNP-SENS and Fast MAS 195Pt Solid-State NMR Spectroscopy. *J. Am. Chem. Soc.* **2020**, *142*, 18936−18945.
(54) Gilbert, T. M.; Ziegler, T. Prediction of ^{195}Pt NMR Chemical Shifts by Density Functional Theory Computations: The Importance

https://doi.org/10.1021/acs.inorgchem.2c00229
Inorg. Chem. 2022, 61, 6888−6897

of Magnetic Coupling and Relativistic Effects in Explaining Trends. *J. Phys. Chem. A* **1999**, *103*, 7535−7543.
(55) Ebsworth, E. A. V.; Rankin, D. W. H.; Cradock, S. *Structural Methods in Inorganic Chemistry*, 2nd ed.; Blackwell Scientific Publications, 1991.
(56) Wang, H.; Liu, J.; Deng, Y.; Min, T.; Yu, G.; Wu, X.; Yang, Z.; Lei, A. Pincer Thioamide and Pincer Thioimide Palladium Complexes Catalyze Highly Efficient Negishi Coupling of Primary and Secondary Alkyl Zinc Reagents at Room Temperature. *Chem.—Eur. J.* **2009**, *15*, 1499−1507.
(57) Liu, J.; Wang, H.; Zhang, H.; Wu, X.; Zhang, H.; Deng, Y.; Yang, Z.; Lei, A. Identification of a Highly Efficient Alkylated Pincer Thioimido−Palladium(II) Complex as the Active Catalyst in Negishi Coupling. *Chem.—Eur. J.* **2009**, *15*, 4437−4445.
(58) Hartwig, J. *Organotransition Metal Chemistry: From Bonding to Catalysis*; University Science Books, 2010.
(59) Ananikov, V. P.; Musaev, D. G.; Morokuma, K. Theoretical Insight into the C-C Coupling Reactions of the Vinyl, Phenyl, Ethynyl, and Methyl Complexes of Palladium and Platinum. *Organometallics* **2005**, *24*, 715−723.
(60) Kameo, H.; Yamamoto, H.; Ikeda, K.; Isasa, T.; Sakaki, S.; Matsuzaka, H.; García-Rodeja, Y.; Miqueu, K.; Bourissou, D. Fluorosilane Activation by Pd/Ni→Si−F→Lewis Acid Interaction: An Entry to Catalytic Sila-Negishi Coupling. *J. Am. Chem. Soc.* **2020**, *142*, 14039−14044.
(61) Schmidt, M. W.; Baldridge, K. K.; Boatz, J. A.; Elbert, S. T.; Gordon, M. S.; Jensen, J. H.; Koseki, S.; Matsunaga, N.; Nguyen, K. A.; Su, S.; Windus, T. L.; Dupuis, M.; Montgomery, J. A. General Atomic and Molecular Electronic Structure System. *J. Comput. Chem.* **1993**, *14*, 1347−1363.
(62) Barca, G. M. J.; Bertoni, C.; Carrington, L.; Datta, D.; De Silva, N.; Deustua, J. E.; Fedorov, D. G.; Gour, J. R.; Gunina, A. O.; Guidez, E.; Harville, T.; Irle, S.; Ivanic, J.; Kowalski, K.; Leang, S. S.; Li, H.; Li, W.; Lutz, J. J.; Magoulas, I.; Mato, J.; Mironov, V.; Nakata, H.; Pham, B. Q.; Piecuch, P.; Poole, D.; Pruitt, S. R.; Rendell, A. P.; Roskop, L. B.; Ruedenberg, K.; Sattasathuchana, T.; Schmidt, M. W.; Shen, J.; Slipchenko, L.; Sosonkina, M.; Sundriyal, V.; Tiwari, A.; Galvez Vallejo, J. L.; Westheimer, B.; Włoch, M.; Xu, P.; Zahariev, F.; Gordon, M. S. Recent Developments in the General Atomic and Molecular Electronic Structure System. *J. Chem. Phys.* **2020**, *152*, 154102.
(63) Becke, A. D. Density-Functional Thermochemistry. III. The Role of Exact Exchange. *J. Chem. Phys.* **1993**, *98*, 5648−5652.
(64) Lee, C.; Yang, W.; Parr, R. G. Development of the Colic-Salvetti Correlation-Energy Formula into a Functional of the Electron Density. *Phys. Rev. B: Condens. Matter Mater. Phys.* **1988**, *37*, 785−789.
(65) Stephens, P. J.; Devlin, F. J.; Chabalowski, C. F.; Frisch, M. J. Ab Initio Calculation of Vibrational Absorption and Circular Dichroism Spectra Using Density Functional Force Fields. *J. Phys. Chem.* **1994**, *98*, 11623−11627.
(66) Stevens, W. J.; Krauss, M.; Basch, H.; Jasien, P. G. Relativistic Compact Effective Potentials and Efficient, Shared-Exponent Basis Sets for the Third-, Fourth-, and Fifth-Row Atoms. *Can. J. Chem.* **1992**, *70*, 612−630.
(67) Ditchfield, R.; Hehre, W. J.; Pople, J. A. Self-Consistent Molecular-Orbital Methods. IX. An Extended Gaussian-Type Basis for Molecular-Orbital Studies of Organic Molecules. *J. Chem. Phys.* **1971**, *54*, 724−728.
(68) Francl, M. M.; Pietro, W. J.; Hehre, W. J.; Binkley, J. S.; Gordon, M. S.; DeFrees, D. J.; Pople, J. A. Self-Consistent Molecular Orbital Methods. XXIII. A Polarization-Type Basis Set for Second-Row Elements. *J. Chem. Phys.* **1982**, *77*, 3654−3665.
(69) Hariharan, P. C.; Pople, J. A. The Influence of Polarization Functions on Molecular Orbital Hydrogenation Energies. *Theor. Chim. Acta* **1973**, *28*, 213−222.
(70) Hehre, W. J.; Ditchfield, R.; Pople, J. A. Self-Consistent Molecular Orbital Methods. XII. Further Extensions of GaussianType Basis Sets for Use in Molecular Orbital Studies of Organic Molecules. *J. Chem. Phys.* **1972**, *56*, 2257−2261.
(71) Huzinaga, S.; Andzelm, J.; Klobukowski, M.; Radzio-Andzelm, E.; Sakai, Y.; Tatewaki, H. Gaussian Basis Sets. In *Gaussian Basis Sets for Molecular Calculations*; Huzinaga, S.; Physical Sciences Data 16; Elsevier: Amsterdam, 1984; pp 27−426.
(72) Groom, C. R.; Bruno, I. J.; Lightfoot, M. P.; Ward, S. C. The Cambridge Structural Database. *Acta Crystallogr.* **2016**, *72*, 171−179.
(73) Bode, B. M.; Gordon, M. S. Macmolplt: A Graphical User Interface for GAMESS. *J. Mol. Graphics Modell.* **1998**, *16*, 133−138.
(74) Edmiston, C.; Ruedenberg, K. Localized Atomic and Molecular Orbitals. *Rev. Mod. Phys.* **1963**, *35*, 457−464.
(75) Webb, S. P.; Gordon, M. S. Molecular Electronic Structure and Energetics of the Isomers of Ti2H6. *J. Am. Chem. Soc.* **1998**, *120*, 3846−3857.
(76) Harris, R. K.; Becker, E. D.; Cabral de Menezes, S. M.; Goodfellow, R.; Granger, P. Nuclear Spin Properties and Conventions for Chemical Shifts. *Pure Appl. Chem.* **2001**, *73*, 1795−1818.

https://doi.org/10.1021/acs.inorgchem.2c00229
Inorg. Chem. 2022, 61, 6888−6897